Supplemental Information for:

Simultaneous Detection of Ozone and Nitrogen Dioxide by Oxygen Anion Chemical Ionization Mass Spectrometry: A Fast Time Response Sensor Suitable for Eddy Covariance Measurements

Gordon A. Novak, Michael P. Vermeuel, Timothy H. Bertram

Department of Chemistry, University of Wisconsin – Madison, Madison, WI, USA

Correspondence to: Timothy H. Bertram (timothy.bertram@wisc.edu)

Component	Voltage (V)
IMR Region (95 mbar)	
IMR	1.5
CDC/ Short Segmented Quadrupole Region (2mbar)	
Lens Nozzle	-1.1
SSQ Entrance Plate	-3.5
SSQ Front	-4.2
SSQ Back	-5.8
Lens Skimmer	-5.7
Skimmer	-3.9
Big Segmented Quadrupole Region (1.2×10^{-3} mbar)	
BSQ Front	-1.0
BSQ Back	-1.0
Skimmer 2	5.0

Table S1: Operational ion optic voltages and chamber pressures for the three front end chambers of the Ox-CIMS. Ion declustering strength is primarily determined by the voltage difference between the Skimmer and BSQ Front. The nomenclature of Brophy and Farmer. (2016) is used for ion optic component labelling.

Reagent Ion	O_2^- (kcal mol^{-1})	CO_3^- (kcal mol^{-1})
H_2O	-18.97	-13.18
H_2O_2	-29.42	-21.15
CH_3OOH	-25.00	-7.92
HNO_3	-26.76	-24.10

Table S2: Calculated binding enthalpies in kcal mol^{-1} for O_2^- and CO_3^- reagent ions to water (H₂O), hydrogen peroxide (H$_2$O$_2$), methyl hydrogen peroxide (CH$_3$OOH), and nitric acid (HNO$_3$) in kcal mol^{-1}. Calculations were performed with the MP2/aug-cc-pvdz-PP theory and basis set.
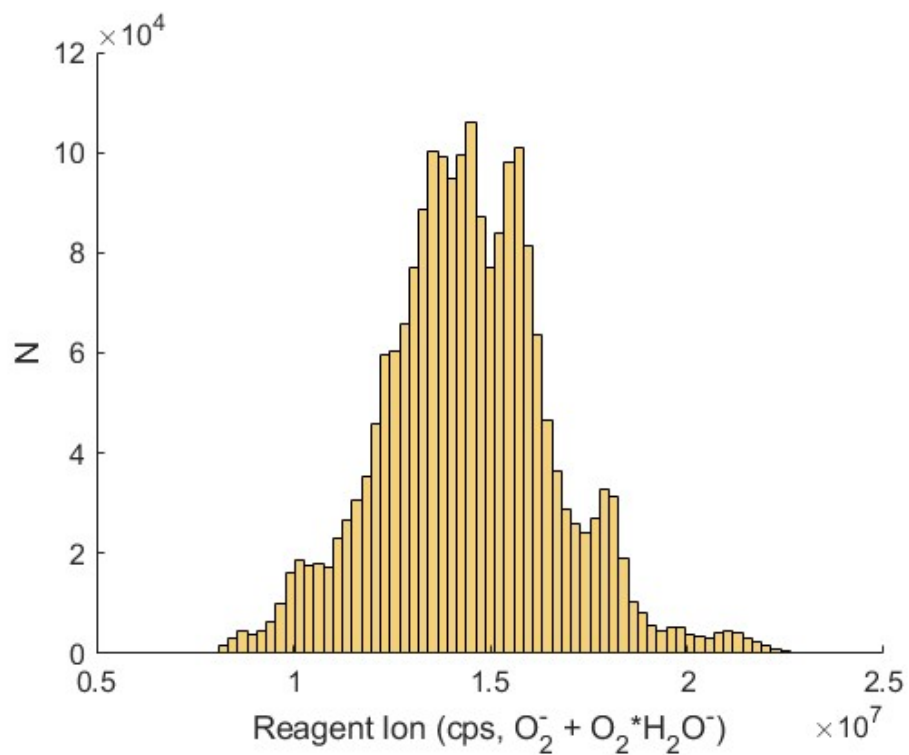
Figure S1: Distribution of 1 Hz reagent ion signal as the sum of O_2^- and $(O_2 \cdot H_2O)^-$ during the full ambient sampling period from Scripps Pier. Absolute sensitivity to O_3 and NO_2 scales directly with the magnitude of reagent ion signal. Mean reagent ion signal during the campaign was 1.45×10^7 cps corresponding to an absolute sensitivity to O_3 and NO_2 of 1.8×10^5 and 1.05×10^5 cps ppbv^{-1} respectively at a specific humidity of 8 g kg^{-1}.

$$y = y_o + A\exp(-Bx)$$

$y0 = 6.62 \times 10^4 \pm 1.1 \times 10^3$

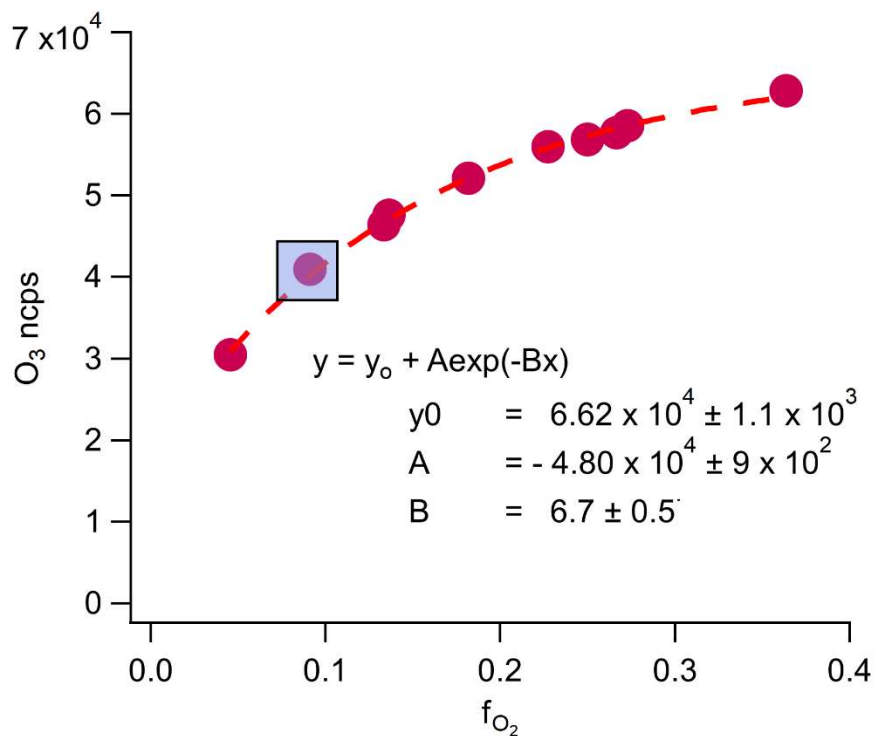$A = -4.80 \times 10^4 \pm 9 \times 10^2$

$B = 6.7 \pm 0.5$

Figure S2: Normalized count rate of background CO_3^- signal at the sum of —m/Q 60 and —m/Q 48 as a function of oxygen fraction in the reagent ion precursor flow (f_{O_2}), with least squares exponential fit line. Reagent ion flow f_{O_2} was varied while the inlet was overflowed with zero air containing 380 ppmv CO_2, to isolate the background production of CO_3^- in the reagent ion generation source. The background O_3 production was 1.5 ppbv at f_{O_2} of 0.08 (blue square overlay) used during ambient sampling.
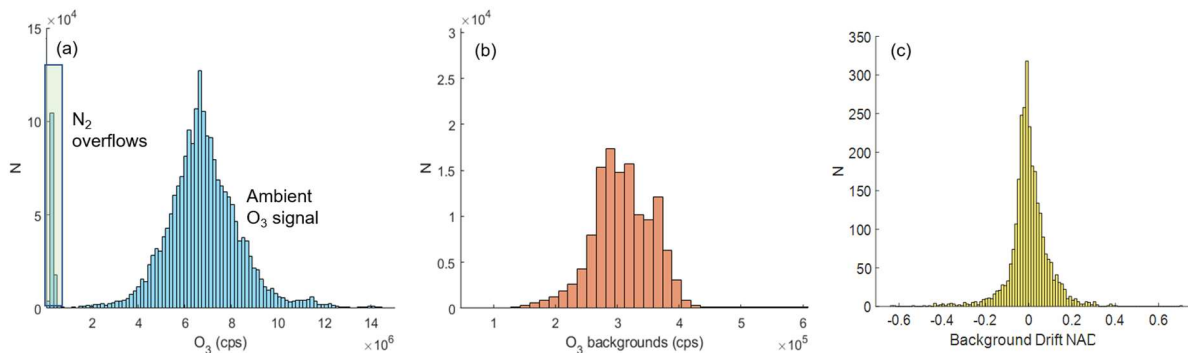
Figure S3: (a) Distribution of observed count rates of the sum of CO_3^- (-60 m/Q) and O_3^- (-48 m/Q) during the full sampling period from Scripps Pier. The green shaded region shows periods of dry UHP N_2 overflow of the sampling line. **(b)** Distribution of observed count rates during dry N_2 overflow periods overflow only. Count rates during overflow periods show high consistency between overflow periods with a mean of 3.1×10^5 and standard deviation of 5.0×10^4 counts per second. Residual CO_3^- during overflow periods is from generation in the reagent ion source rather than off gassing from instrument surfaces. **(c)** Distribution of normalized adjacent differences of the mean summed CO_3^- and O_3^- signal during each three-minute overflow period. The NAD of overflow periods is a measure of point to point stability of the background over the full campaign. The 1 σ deviation of the NAD distribution is 9% which gives an upper limit of the variability between subsequent O_3 backgrounds. A 9% variability in the background corresponds to 110 pptv O_3 at mean overflow signal of 3.1×10^5 cps.
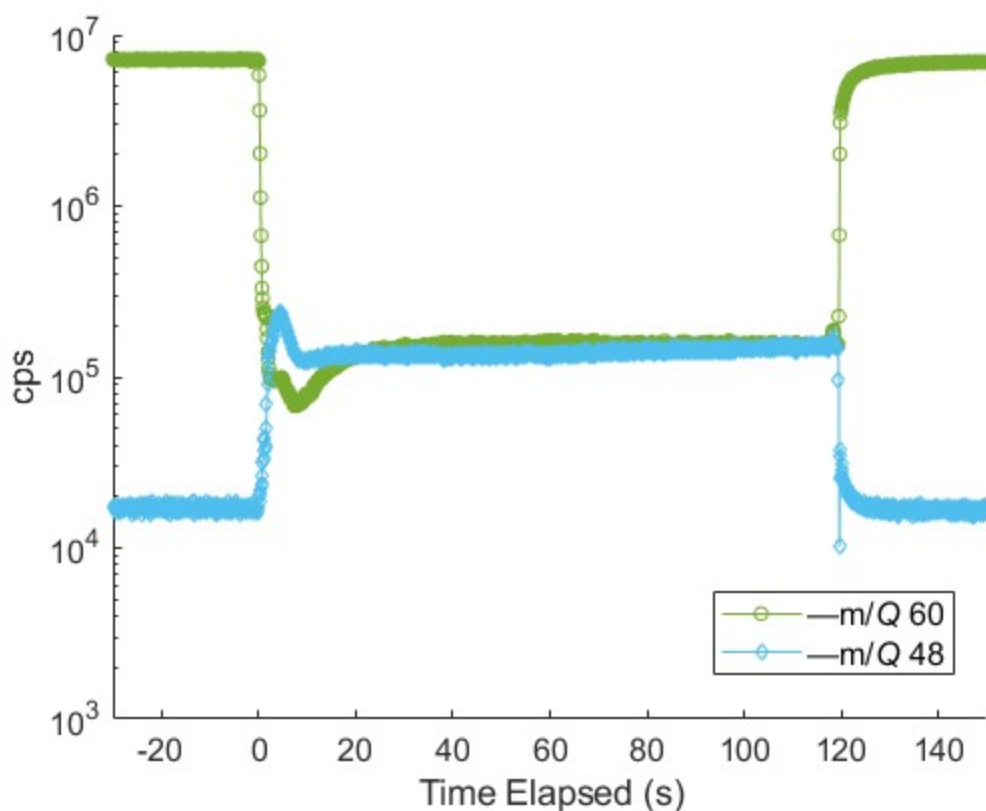
Figure S4: Background count rate of ozone detected as CO_3^- at —60 m/Q and as O_3^- at —48 m/Q during an N₂ overflow background determination period during ambient sampling at Scripps Pier. Overflow of dry N₂ was started at 0 s and stopped at 120 s. During N₂ overflow periods during field sampling, no CO₂ was added to drive the reaction product to CO_3^-. This leads to the detection of a portion of the O₃ background signal as O_3^- during N₂ overflow which must be accounted for. Count rates of O_3^- were of similar magnitude to the CO_3^- signal during N₂ overflow periods during field sampling. From lab calibrations the sensitivity to O_3^- at 0 ppmv CO₂ and 0 g kg⁻¹ SH is approximately a factor of three higher than CO_3^-. Accounting for the background signal at O_3^- increases the mean O₃ background during field sampling by 0.6 ppbv (from approximately 0.7 to a 1.3 ppbv total O₃ background).
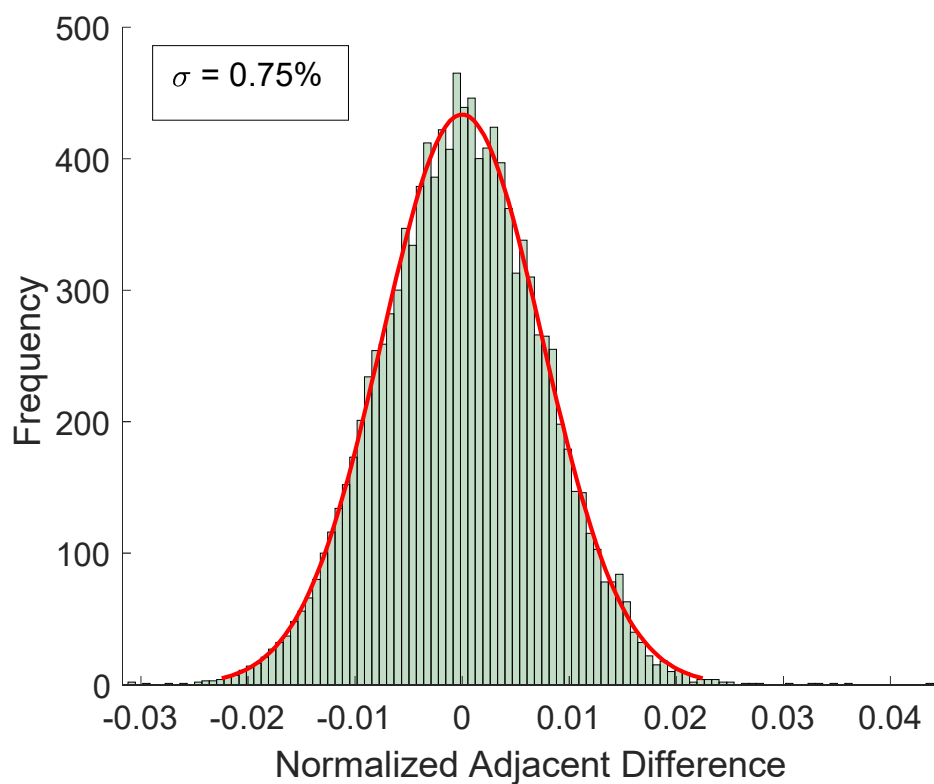
Figure S5: Distribution of normalized adjacent differences of 10 Hz O$_3$ signal during a 2-minute dry N$_2$ overflow period during ambient sampling at Scripps Pier. The 1σ upper limit of precision is 0.75% corresponding to 7.5 pptv precision in the 1.3 ppbv background O$_3$ signal. Precision limitations from background O$_3$ generation in the ion source are unlikely to be significant in the overall precision of the instrument during ambient sampling where precision is 300 pptv at 40 ppbv ambient O$_3$ concentrations.
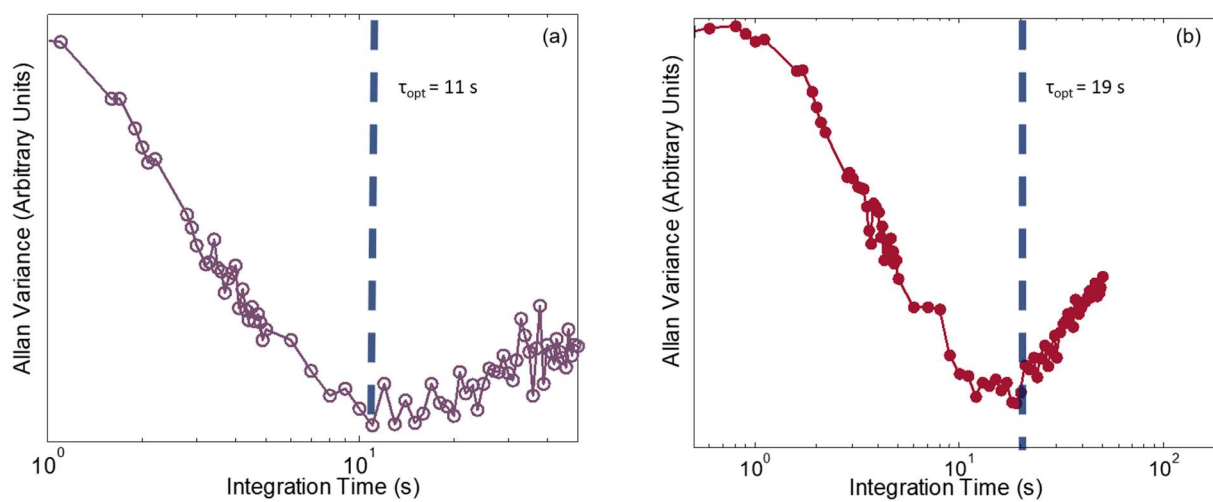
Figure S6: Allan variance determination of optimal averaging time for (a) O_3 and (b) NO_2 for sampling of a constant calibration source in lab for approximately 10 minutes with 10 Hz data collection. The minimum of the Allan variance curve is the optimum averaging time (τ_{opt}) that results in the lowest achievable LOD. For O_3 τ_{opt} was 11 s, and for NO_2 τ_{opt} was 19 s.
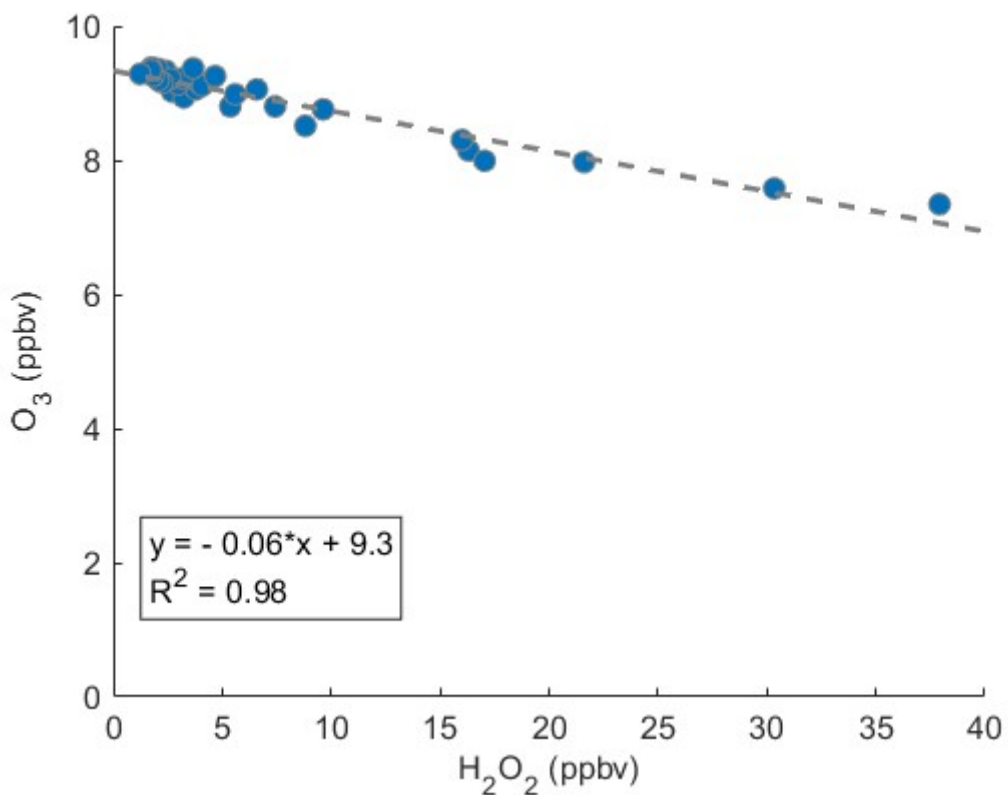
Figure S7: Regression of O₃ signal against H₂O₂ from laboratory sampling of approximately 8 ppbv O₃ with fast introduction of a H₂O₂ source up to 40ppb. Linear regression shows a loss of 0.06 ppbv of the O₃ signal per ppbv H₂O₂ added. H₂O₂ is detected as an adduct with O_2^- the parent ion $H_2O_2^-$ at —m/Q 66. The CO_3 $(H_2O_2)^-$ adduct at —94 m/Q is observed respond with increase with H₂O₂ introduction but has a persistent high signal which is attributed to a ubiquitous $O_2(CO_2)(H_2O)^-$ adduct.
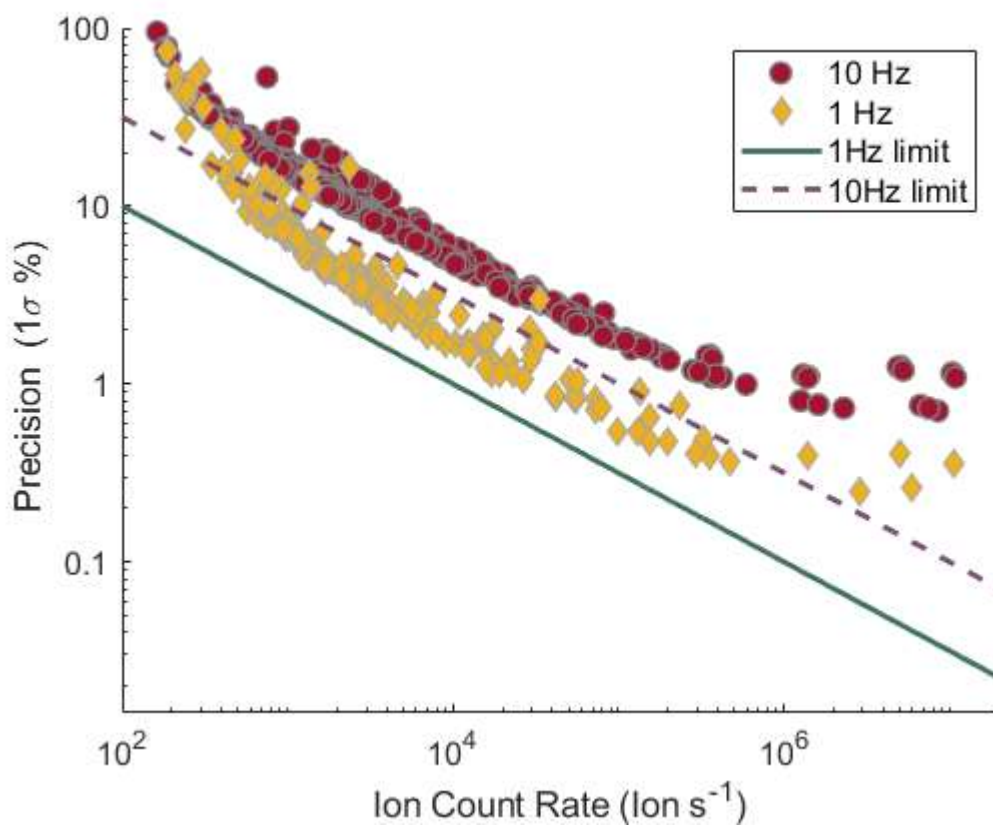
Figure S8: Short-term instrument precision from distribution of normalized adjacent differences against ion count rate for 10 Hz and 1 Hz data averaging. Normalized adjacent differences were calculated for all masses -30 to -250 m/Q for a 27-minute ambient sampling period. Precision is reported as 1σ of the NAD distribution for each mass. Ion count rates are the mean unnormalized count rate over the 27-minute sampling period.
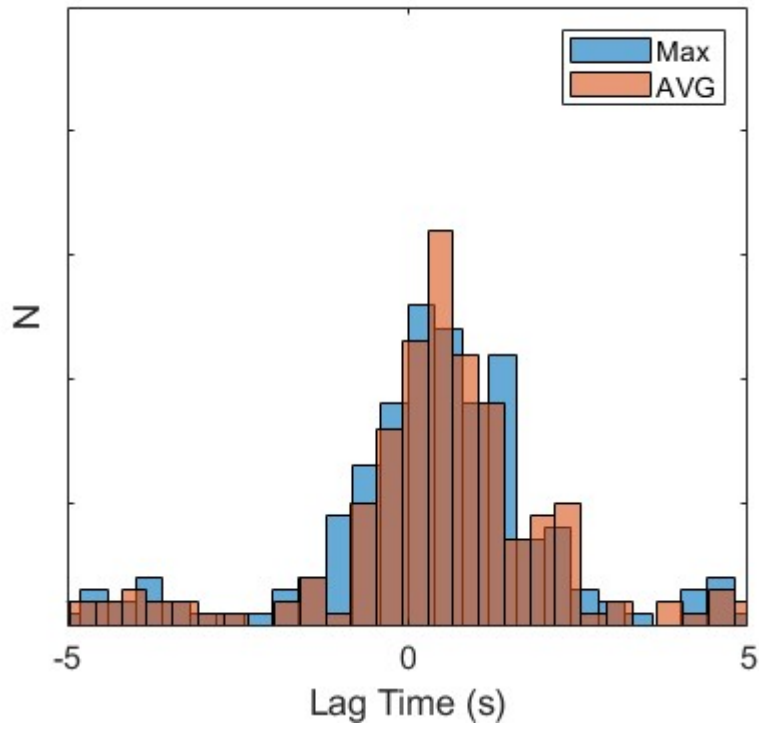
Figure S9: Histogram of determined lag times determined as the maximum (MAX) absolute magnitude of the autocovariance and from the maximum absolute magnitude of a 10 point moving median (AVG) of the autocovariance over a ±5 s lag window.
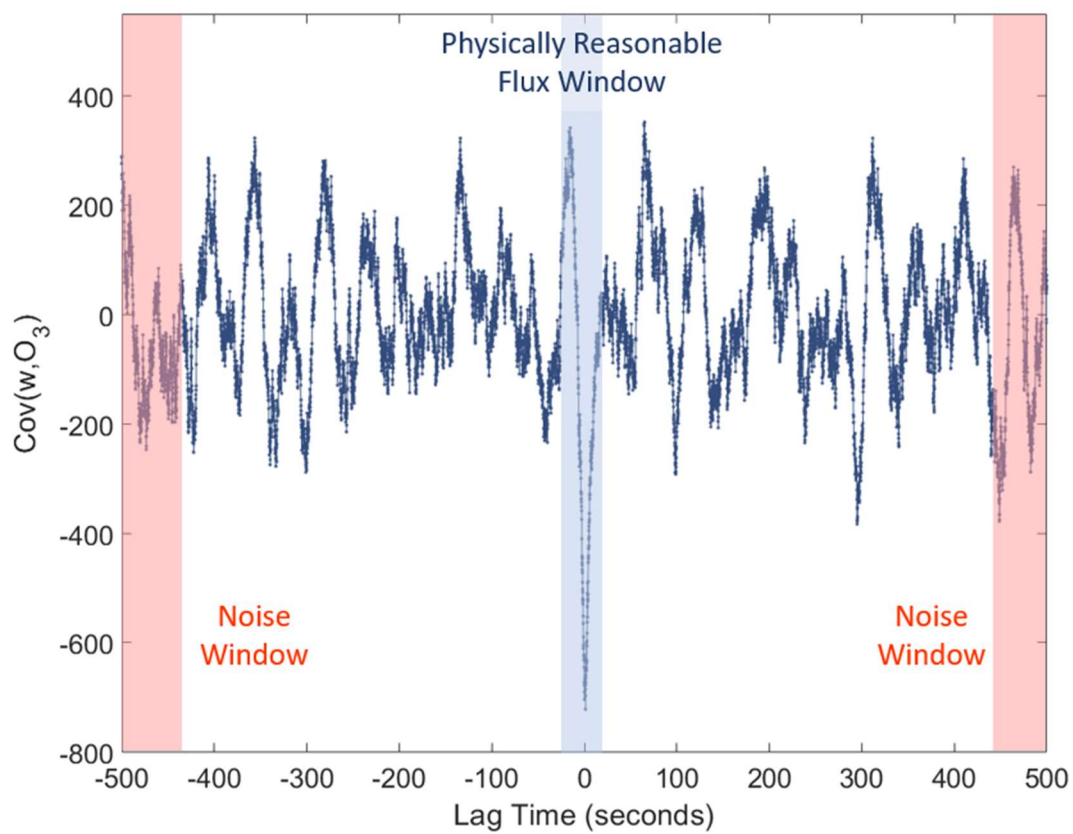
Figure S10: Calculation of cross-covariance at very long lag times (-500 to -485 & 485-500 s) used to determine the flux LOD via the LOD_{RMSE} and LODσ methods. Covariance in the physically reasonable flux window of lag times (-3 to 3 s) is well resolved from the covariance magnitude at long lag times driven by noise.
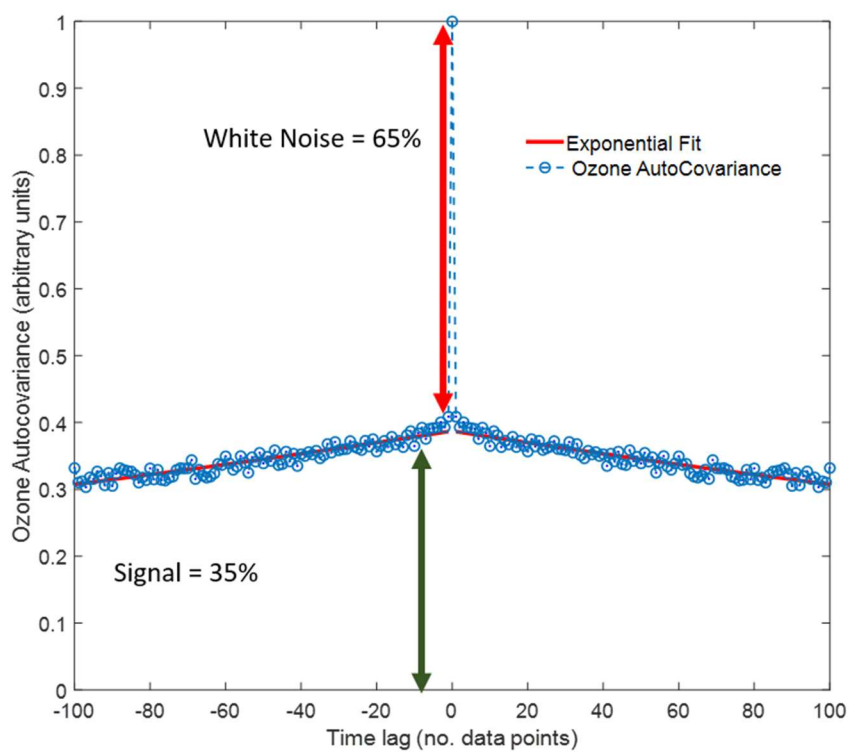
Figure S11: Ozone auto-covariance for 10 Hz O$_3$ signal for a single flux averaging period. White noise only contributes to the auto-covariance at a lag of 0 points. Auto-covariance at other lag times is from real long-term coherence in the signal, either from atmospheric variability or instrument drift.
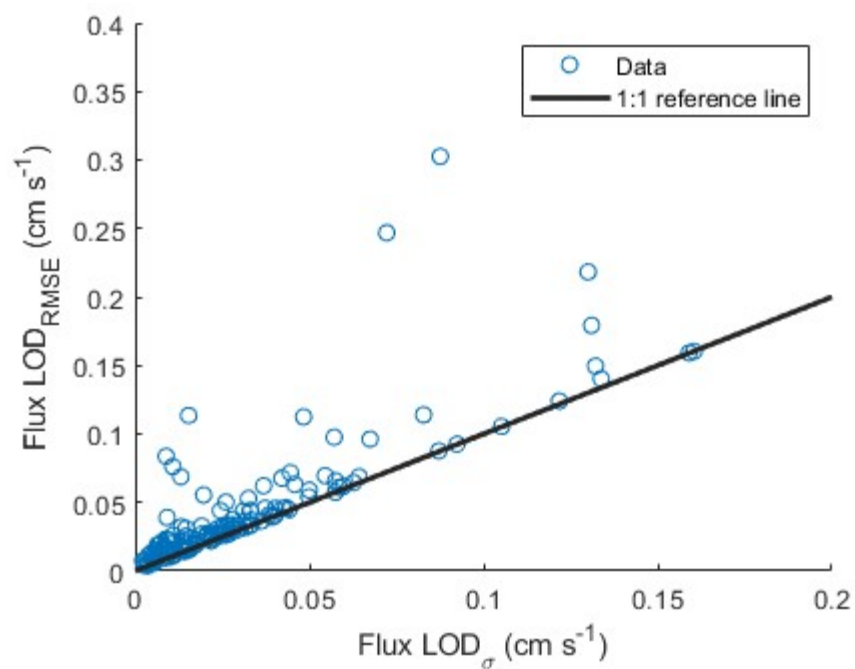
Figure S12: Ozone flux limit of detection from for 27-minute flux periods determined by the LOD$_{RMSE}$ and LODσ methods.

References

Brophy, P. and Farmer, D. K.: Clustering, methodology, and mechanistic insights into acetate chemical ionization using high-resolution time-of-flight mass spectrometry, Atmos. Meas. Tech., 9(8), 3969–3986, doi:10.5194/amt-9-3969-2016, 2016.